Youssef *et al.*
Journal of Engineering and Applied Science (2024) 71:53
https://doi.org/10.1186/s44147-024-00380-3

Journal of Engineering and Applied Science

RESEARCH Open Access

Shear capacity of miniature beams with continuous staggered spiral stirrups

Ahmed Youssef[1*], Shereen Mawaad[1,2] and Hamed Salem[1]

*Correspondence:
ahmedyoussef@cu.edu.eg

[1] Department of Structural Engineering, Cairo University, Giza, Egypt
[2] Institute of Aviation Engineering and Technology, Giza, Egypt

Abstract

Scaled-down-reinforced concrete beams with rectangular staggered continuous spiral stirrups are experimentally investigated. Scale-down RC beams were considered in the current research due to ease of construction and economic feasibility. As the brittle shear failure should be avoided, continuous research trials have been conducted to find an effective technique to improve shear failure mechanism. Twenty-two beams were investigated for shear behavior under 4-point static push-over load considering the normal stirrups and compared with continuous staggered spiral ones. Stirrup spacing, shear arm ratio a/d, and shear reinforcement configurations are the main variables. All beams were designed and scaled down to be one-eighth of the full-scale beams. To minimize the size effect of using small-scale models, mortar was used instead of conventional concrete. The focus in this study was related to improved shear capacity, dissipated energy, and shear cracks propagation. It was found that using spiral reinforcement instead of normal one leads to a significant enhancement in shear capacity and dissipated energy by 33% and 45%, respectively. Therefore, the prototype RC model expected capacities were detailed calculated considering the scale-down factor used by authors. The experimental results were compared by calculated values according to international standard and specifications.

Keywords: Scale-down modelling (SDM), Reinforced concrete (RC), Reinforcement (RFT), Shear span arm ratio (a/d)

Introduction

Shear failure is a brittle failure that must be avoided in order to boost structural ductility. Shear failure generates catastrophic failures; this rapid failure mode necessitated the examination of more efficient methods of designing these beams for shear. Experimental scale-down models play a substantial part in structural engineering. Prototype investigation is frequently wasteful or impractical. Reduced-scale models are a good way to study the structure behavior. There are numerous benefits to scale modelling, the most important of which is the efficiency of cost, labor, and time when preparing the steel cage, which results in an increased demand for scale-down modelling "Seo (2000) and Mahmoud (2022) [1, 2]." The change in strength caused by a change in sample size is referred to as the size effect. As the sample size decreases, the measured nominal strength increases "Majorana (2015) [3]." "Mohamed (2012) [4]" tested this theory

through studying the size effect and examining the miniature pile. As the member size was reduced and the nominal resistance to shear was higher, as contradicted to flexure, he used mortar to overcome the size effect by reducing the shear transmission along the crack. The Buckingham Pi hypothesis has been the most commonly used in dimensional analysis to generate a similarity relationship. "Carpinteri (2010) [5]," for instance, studied the structural mechanism of RC beams exposed to shear effect. The proposed model was based on several geometrical and mechanical parameters. "Christianto (2020) [6]" further investigated the sample size through a cylinder and a beam with diverse height. His outcomes confirm that shear is affected by sample size. The higher the beam depth, the lesser the shear stress. Shear strength is influenced by reinforcement ratio, concrete tensile strength, and the presence of aggregates, section size, and shear span (a/d). He found that the size effect can be described by the difference in sizes and scales with the preservation of the geometric dimensions as well as the preservation of the shear arm and the same reinforcement ratio. A continuous spiral is used to overcome the drawbacks of separate ties; it highlights the significant contribution of the web RFT towards shear capacity, which is proportional to shear reinforcement intervals and its span depth ratio. Various studies were conducted addressing this topic, for instance, "Shatarat (2016) [7]" investigated 28 RC beams under 4-point static load using continuous spiral ties as transverse RFT, where he examined five inclination angles of ties, three intervals, and two shear arm ratios. To implement spiral ties, Shatarat recommended the ACI design shear formula to boost the shear strength and ductility. Similarly, "Joshy (2017) [8]" investigated 12 RC beams in a 4-point static load through spiral ties in self-compacting, using intervals as variables. As a result, he found that continuous spiral ties are better in preparing steel cages compared to separate ties in terms of speed, high ductility, and shear capacity, and that SCC can produce a more favorable critical crack evolution. Furthermore, "Megahid (2016) [9]" examined the impact of shear arm ratio a/d on the mechanism of an HSCB exposed to point load, where he studied the impact of shear arm ratio, concrete grade, and stirrups spacing; his test program comprised 24 full-scale-rectangular HSCB, and his outcomes were in line with various codes and formulas. "Hua (2018) [10]" investigated experimentally eleven RC beam to estimate the shear strength participated by stirrups and concrete. He found that the structural variables were transverse RFT sort (plain round or deformed bar) and diverse with an a/d ratio. "Meghana (2018) [11]" distinguished the RC beams performance reinforced with diverse forms of continuous spiral stirrups. As a result, cost reduction through the implement of continuous spiral is regarded as a significant advantage. "TalapaReddy (2020) [12]" discussed the confinement steel influence on flexural mechanism of RC beams exposed to monotonic loading. Separate ties, inclined ties, rectangular spirals, and lacing are all considered as confinement patterns Based on the findings, it was determined that inclined ties and lacing have higher ductility than separate ties and rectangular spirals. "Dewi (2020) [13]" tested nine RC beams with circular cross sections for assessing the shear mechanism. The test parameters were the reinforcement ratio and stirrup kinds. The outcomes revealed that all samples without ties were fallen due to shear force. The beams with spiral ties were slightly more ductile. "Azimi (2016) [14]" boosted the RC columns performance for seismic in terms of energy dissipation capacity and ductility by applying continuous spiral ties. A new suggested beam-column assembly, "twisted

opposing rectangular spiral," was conducted numerically and experimentally. Finally, the outcomes showed that the new suggested connection has improved ultimate lateral resistance, energy dissipation capacity, and ductility. In this study, staggered continuous spiral as transverse RFT was found to affect the shear behavior of the miniature under 4-point static push over load. Furthermore, the staggered spiral's continuity contribution to shear strength and miniature mechanism was tested and discussed. This article focuses on assessing the contribution of spiral ties to the shear capacity based on the monitored test results. The design requirements of "ACI Code (2019) [15], Japanese Standards (2007) [16] Euro code (2005) [17], Zararis (2003) [18], and Niwa model (1986) [19] model" were applied in this research to assess the shear strength.

Research significance

The shear behavior of scaled-down beams reinforced with staggered rectangular continuous spiral stirrups is investigated in this study. Twenty-two rectangular-section one-eighth scale beams are used in the experiment. The structural parameters investigated were as follows: (1) stirrup's arrangement as transverse shear RFT (normal rectangular stirrups — staggered rectangular spiral stirrups), (2) stirrups spacing (30–40–50–60–90 mm), and (3) the shear arm ratio (1, 1.5, 2, 2.5, 3, 3.5). All miniatures had identical concrete strength and reinforcement. The current study employed the scaled-down model, which has received considerable attention in the literature and has been moderately validated for shear problems. The target of this study was to evaluate the efficiency of spiral stirrups on the shear behavior through load–deflection curves, crack propagation, and failure modes were evaluated.

Experimental

Set up for testing

Concrete Research Modelling Laboratory at Cairo University tested test miniatures. A 25-kN load cell was applied to estimate the implemented load. A spreader beam was placed on two roller supports to convey the load to miniatures as revealed in Fig. 1. Hence, once the load cell pushes over the spreader I beam, the end support will receive

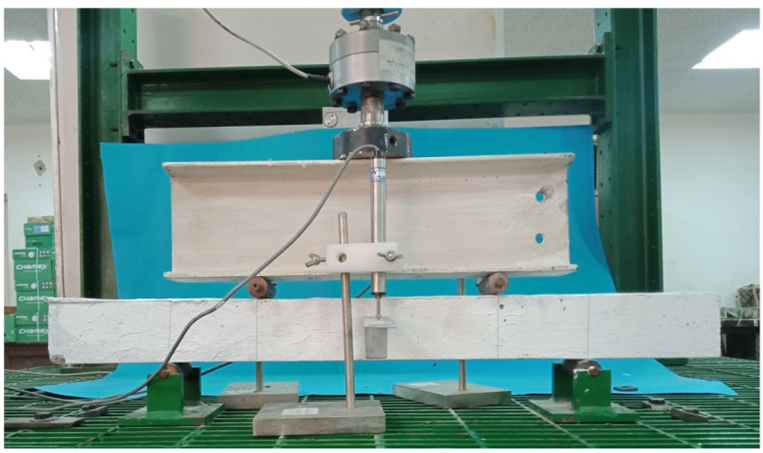

Fig. 1 The set up for the shear test

half the load. According to the Egyptian code [20], the miniatures were designed ties spacing and shear arm ratio a/d, and stirrup configurations were the structural parameters. Two-point loads were applied to the spherical plate, then the spreader steel beam, and finally the miniature. Three linear variable deflection transducers (LVDTs) were used to measure the deflection of each miniature at the 2-point load and at mid-span. Incremental loads, crack propagation, and failure mode were recorded thru the test. The outcomes were depicted to evaluate the shear capacity of (RC) beams.

Miniatures details

The experimental study focused on the shear behavior of miniature beams under monotonous loads. The study comprised investigating 22 RC beam miniatures with rectangular cross sectional of 50×75 mm. The miniature length is 800 mm, and all tested beams had an investigated span of 500 mm. The miniature beams were reinforced with 6ϕ4 bottom and 2ϕ3 top as longitudinal RFT. The upper and lower RFT bars of all beam's miniatures were hooked down and up beyond the supports to prevent anchorage slippage. Table 1 displays the parameters of studied stirrups spacing models with unchanged $(a/d) = 2.6$. Table 2 displays the parameters of studied shear span arm ratio (a/d) models with unchanged stirrup spacing 30 mm.

Miniatures mixture

The cementations mortar mix was designed to manufacture mortar with strength of 40 Mpa at 28-day cubic compressive strength. The ratios of mortar mix were presented in Table 3. A mortar mixer merged natural sand, ordinary Portland cement, and water, while the mixing time was estimated 5 min. Steel molds were used, and their interiors were oil coated before casting. A vibrator compacted the mortar. After 24 h, the steel mold was removed and continue curing on a daily basis for 28 days. Free cutting steel bars were used as the main reinforcement. Figure 2 represents the fine aggregate grading.

Free cutting steel bar

Free cutting steel bars were plain round smoother than deformed rebar, but they were shorter in length, in addition to passing through stages of processing that make it smooth, where it is grinded or sanded to be smooth. Free cutting steel rods were 2000

Table 1 Parameters studied for stirrups spacing miniatures

Specimen	Stirrup spacing (mm)	Type of transverse RFT
B1	30	Normal stirrups
B2	40	
B3	50	
B4	60	
B5	90	
B6	30	Spiral stirrups
B7	40	
B8	50	
B9	60	
B10	90	

Table 2 Parameters studied for shear span arm ratio (a/d) miniatures

Specimen	Shear span arm ratio (a/d)	Type of transverse RFT
B11	1	Normal stirrups
B12	1.5	
B13	2	
B14	2.5	
B15	3	
B16	3.5	
B17	1	Spiral stirrups
B18	1.5	
B19	2	
B20	2.5	
B21	3	
B22	3.5	

Table 3 Characteristic of mortar mix of miniature beams

W/C %	Sand %	Unit volume kg/m^3		
		Water	Cement	Sand
41.0	100.0	340	820	1012

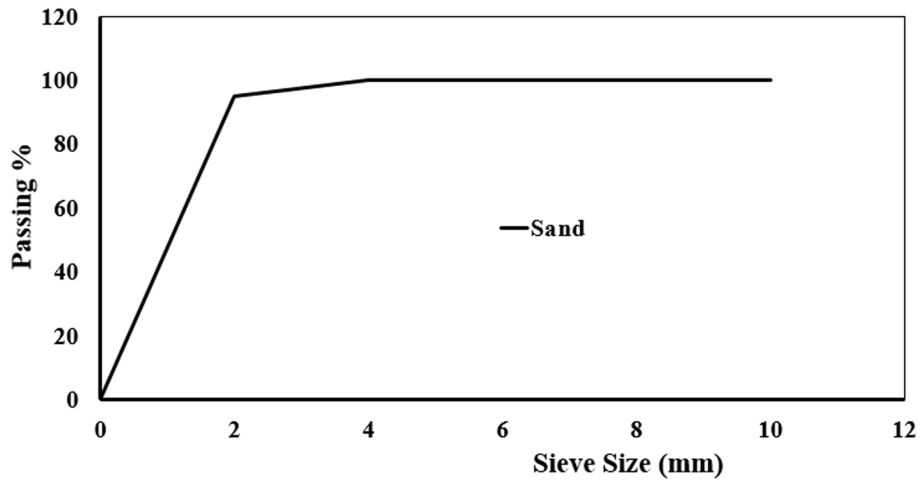

Fig. 2 Depicting fine aggregate grading

mm in length, with different diameters. It is notice that the Young's modulus of free cutting steel is less than the usual value of reinforcing steel and reach about a quarter of the value as a result of the nature of the components of the mixture of these bars and their carbon percentages. These values are from the bar tensile tests in the laboratory. Table 4 displays the free cutting steel characteristics used for the miniature. The stress-strain curve for 2-mm bar diameter and 4-mm bars diameter is shown in Fig. 3. Figure 4 shows the miniature's RFT cage for normal and spiral stirrups.

Table 4 Free cutting steel bars mechanical properties

Diameter (mm)	Area (mm^2)	Young's modulus	Yield stress (N/mm^2)	Ultimate stress (N/mm^2)
4.0	12.57	50 GPa	690	766
3.0	7.10		800	868
2.0	3.14		744	828

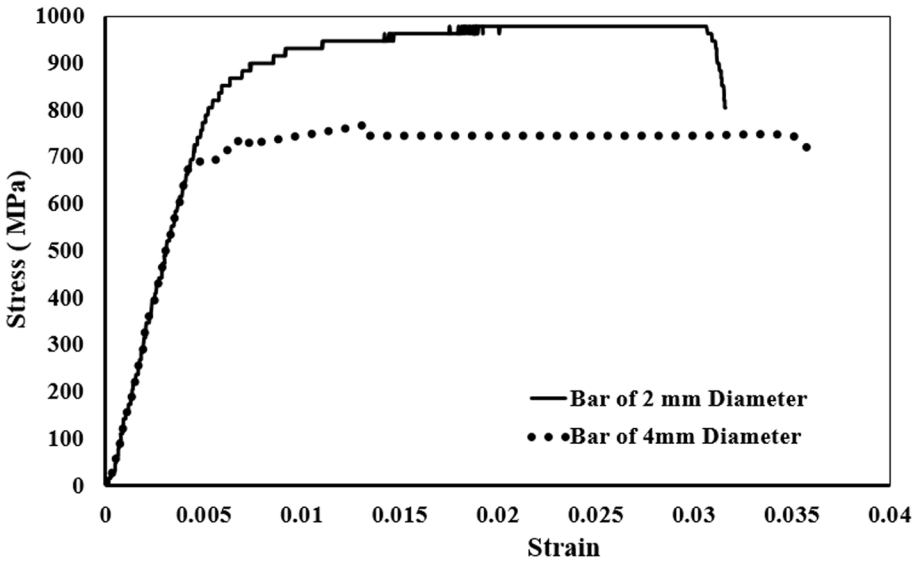

Fig. 3 The stress strain for 2-mm diameter and 4-mm diameter

Fig. 4 The miniature's RFT cage for normal and spiral stirrups

Results and discussion

The results of RC beams, comprising their shear load–deflection curve, crack propagation, and dissipated energy for each miniature beam.

Shear load–deflection curve for diverse stirrup spacing

Figures 5 and 6 illustrate the shear load–deflection curve for the normal stirrups and continuous staggered rectangular spiral with different stirrup spacing (30, 40, 50, 60, and 90 mm), where a/d is kept constant 2.6. The outcomes confirm that the staggered spiral stirrups have a significant influence on the miniature's shear capacity. The shear capacity obtained for miniature B1 reinforced with normal stirrups at spacing 30 mm was 9

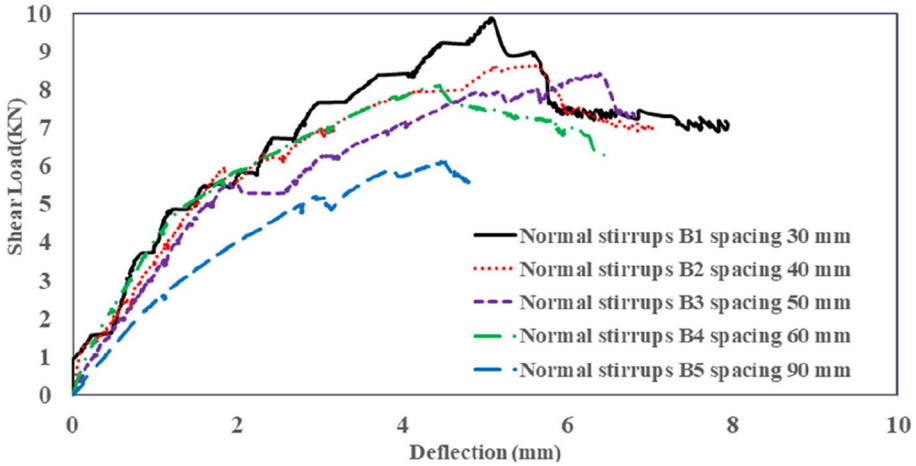

Fig. 5 The shear load–deflection curve of normal ties with various spacing

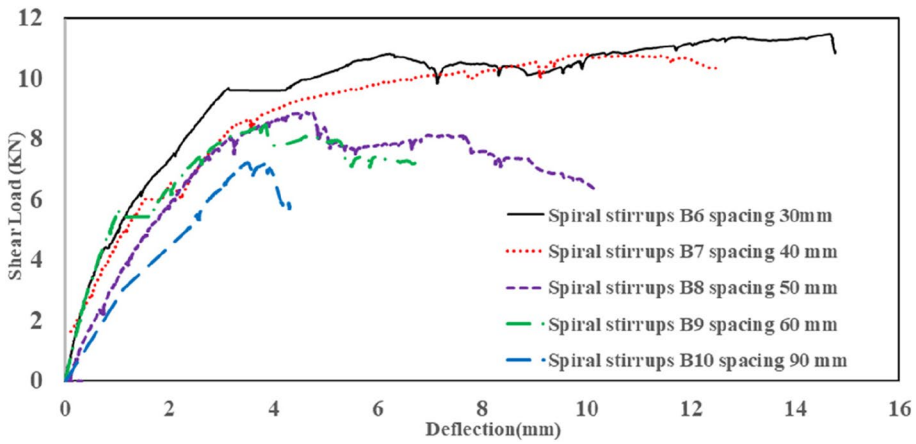

Fig. 6 The shear load–deflection curve of spiral ties with various spacing

kN, with a deflection at peak load of 5.8 mm. The maximum shear capacity obtained for miniature B6 reinforced with staggered rectangular spiral stirrups was 11.7 kN, with a deflection at peak load of 16 mm. The shear capacity increased once spacing decreased. The mechanism of shear load–deflection curves for all models followed the same manners up to first cracking load. All miniature beams performed similarly prior to cracking until the onset cracking load, and then the mechanism changed with different load capacities. Shear strength was higher in spirally staggered miniatures than in normal stirrup miniatures. When spirally miniatures are used instead of normal stirrups, the peak load increased by about 33%. The load and deflection curve clearly demonstrated that the closer the spiral spacing, the higher the miniature capacity, and the bigger the area under the curve. When normal stirrups were used for miniature B5 and the stirrup's spacing was 90 mm, the shear strength reached 4 kN, and also, the deflection at max load decreased until 4 mm. On the other hand, when spiral stirrups were used for miniature B10 and the stirrup's spacing was 90 mm, the shear strength reached 5 kN, and also, the deflection at max load decreased to 5.5 mm. Shear capacity increased significantly

when continuous staggered spiral stirrups were used. This indicates that the closer the ties spacing, the more their efficiency of closing the diagonal shear crack. Given that both are capable of retarding shear failure, the closer the stirrups are spaced, the better the deformations.

Shear load–deflection curve for diverse shear arm ratio

Figures 7 and 8 represent the shear load–deflection curve for normal stirrups and continuous staggered rectangular spiral stirrups with different shear arm ratio (1, 1.5, 2, 2.5, 3, 3.5), where stirrups spacing is kept constant 30 mm. It is obvious that as a/d decreases, the shear capacity increases. The shear capacity for miniature B11 reinforced with normal stirrups is 21 kN, with a deflection at peak load of 5 mm. Miniature B17 reinforced with staggered rectangular spiral stirrups has the highest shear capacity of 23 kN and a deflection at peak load of 9 mm When normal stirrups were used for miniature B16 and the a/d = 3.5, we found the shear strength, it decreased until it reached 6 kN, and also, the deflection at peak load reached 9 mm. On the other hand, when spiral stirrups were used for miniature B22 and the a/d = 3.5, we found the shear strength decreased until it reached 8 kN, and also, the deflection at peak load increased to 10 mm. Shear capacity increased significantly when continuous staggered spiral stirrups were used. Pure shear failure is acquired in the beam miniature with a small a/d ratio, but flexural shear failure is acquired in the beam miniature with a higher a/d ratio.

Cracking propagation

Cracking propagation for diverse spacing with normal stirrups

Figure 9 shows the cracking propagation at peak load for miniatures with diverse stirrup's spacing (B1, B2, B3, B4, and B5), respectively. For miniature B1 of spacing 30 mm,

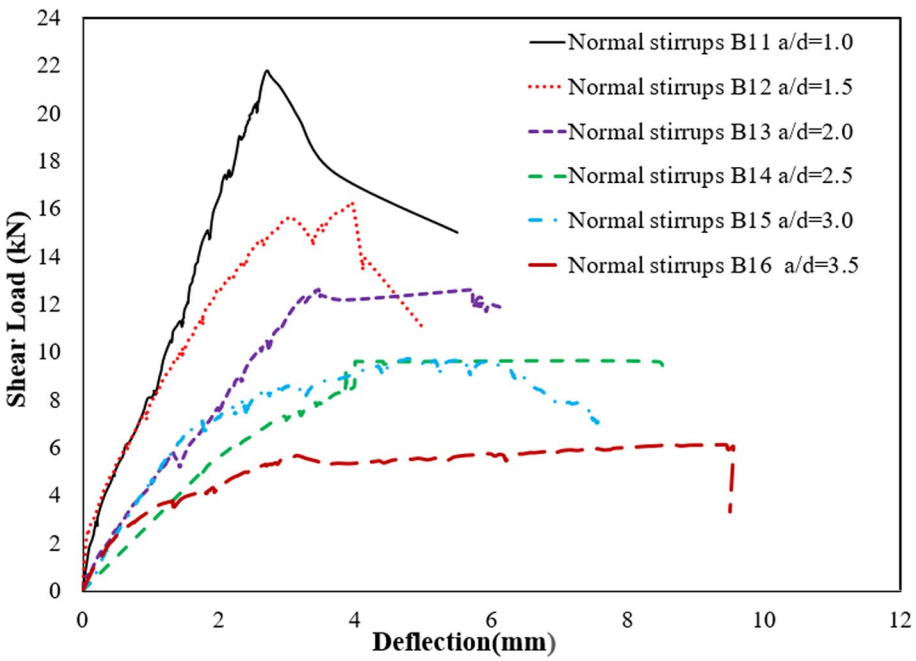

Fig. 7 The shear load–deflection curve of normal stirrups with changed a/d

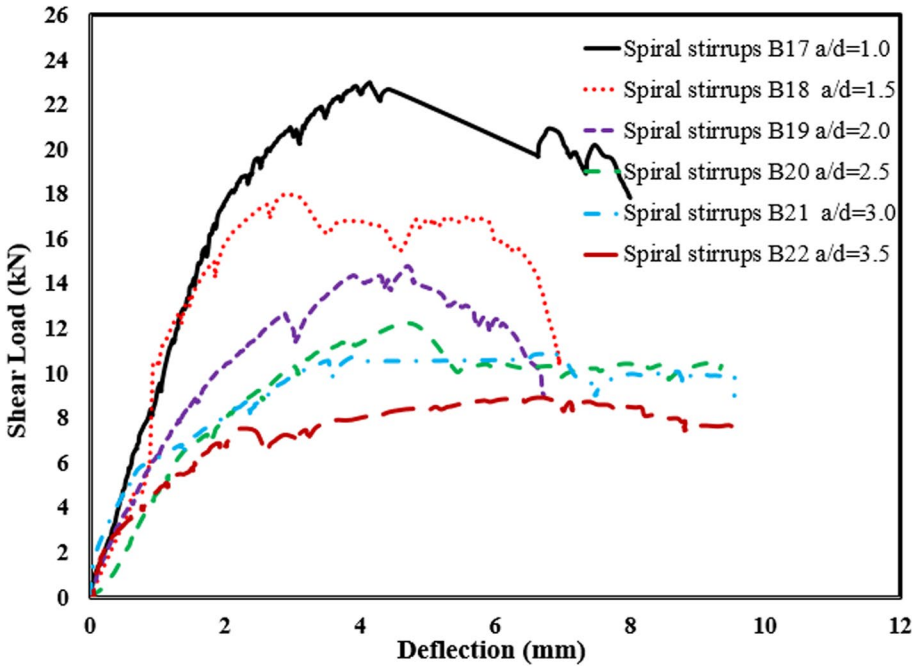

Fig. 8 The shear load–deflection curve of spiral stirrups with changed a/d

at $F=4$ kN, the first flexural crack can be noticed. Up to $F=5$ kN, these cracks stretched in length, but the crack width slowly increased. At $F=7$ kN, vertical flexural crack directly under point load due to slippage of bar. Eventually, inducing end-anchorage failure at peak capacity of 9.5 kN, which induced the concrete to split along the longitudinal RFT at the end of the free cutting steel bar. When the longitudinal RFT is not adequately anchored beyond the crack, this condition occurs. Slippage will occur as a result of this type of end anchor failure, resulting in crack expansion and increased deflection. Direct failure is induced by the sliding of the reinforcing bar relative to the edge. The

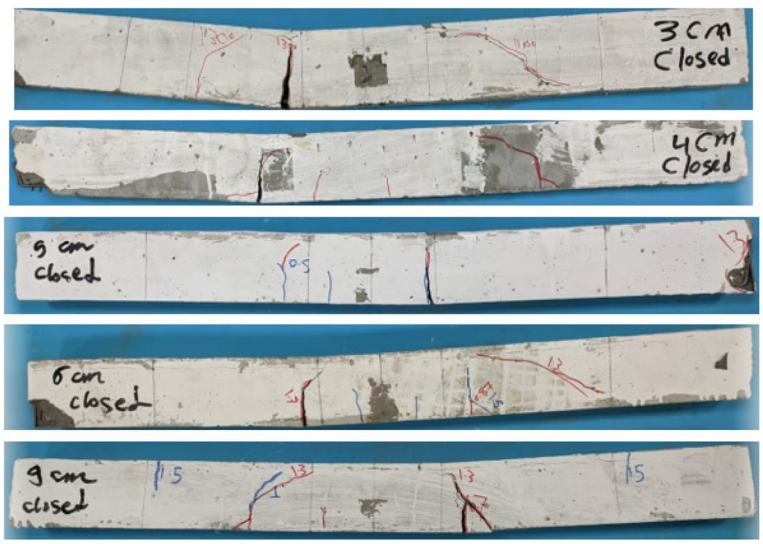

Fig. 9 Cracking pattern of normal stirrups for B1, B2, B3, B4, and B5

failure cannot be overcome because the smooth steel bar has no friction, interlocking, or low adhesion. Increased slippage occurs as a result of the lack of frictional interlocking between the concrete and deformation of the steel bar surface. There is a large deflection and a wider crack width. Because of the low bond strength, the final anchorage is in the form of stirrups. The beam collapses immediately due to the steel sliding relative to the concrete. When the pullout is exceeded and extended to the end of the anchored steel bar, the joint will fail completely. The development length has a significant impact on reinforcing bar pullout. Due to the weak bond strength, the final anchorage is provided in the form of hooks.

Cracking pattern for diverse spacing with continuous spiral stirrups

Figure 10 shows the cracking pattern at peak load for specimens with diverse stirrup spacing (B6, B7, B8, B9, and B10), respectively. For smaller spacing, the staggered spiral stirrups efficiently closed the crack. For stirrup spacing of 30 mm, cracking started as a hair diagonal crack at tension side at a load of 6 kN, and with the loading increase, a diagonal crack propagated towards the beam face. Further loading created another diagonal crack that propagated towards the compression side, eventually causing compression failure at peak capacity of 11.7 kN. The test displayed a clear shear failure mechanism. Diagonal cracks were created in the miniature shear span and lead to shear failure. The inclination angle of cracks was smaller than that of the separate stirrups; hence, a larger shear surface is achieved. The staggered spiral ties helped reaching more ductility and provided higher shear capacity.

For specimen of B10, the photo displays the crack propagation pattern using spiral staggered ties. The first diagonal crack was visible at a load of 4 kN. Up to 5kN, the length of these cracks increased, but the width of the crack slowly increased. At 5.5 kN, shear crack began to manifest in shear zone. With the load increases, the shear crack propagated upward the loading point at a reduced angle. At 7-kN load, the shear crack had been formed at branches. Then the diagonal crack propagated to the compression zone and cracks caused splitting above the support. At failure, the shear reinforcement

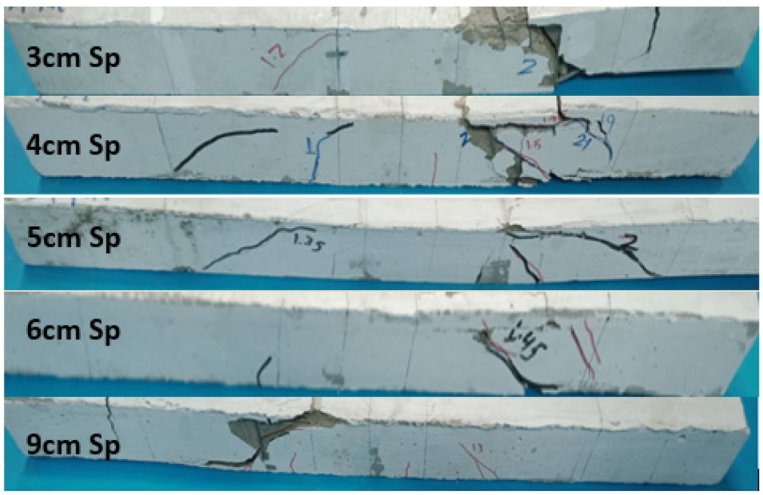

Fig. 10 Cracking propagation of staggered spiral for B6, B7, B8, B9, and B10

yielded. Crack propagation on sides of the miniature was proven to be identical during the test process. The bigger the stirrup spacing, the crack is localized crack.

Cracking pattern for diverse a/d with normal stirrups

Figure 11 shows the cracking pattern at peak load for specimens reinforced with separate ties with diverse a/d (B11, B12, B13, B14, B15, and B16), respectively. When the specimen is loaded about to 45% of the peak load, one inclined diagonal crack, within the shear span, would unawares be widen at the diagonal crack and indicates that shear failure has occurred. The critical diagonal crack extended towards the load point and penetrated the web and rapidly got wider as the beam deflection increased. The shear failure happened once the concrete reached its maximum strength, when it reaches the compression shear zone. Diagonal cracks (flexural-shear cracks or web-shear cracks) occurred first and extended in the shear arm.

Cracking pattern for diverse a/d with continuous staggered spiral stirrups

Figure 12 shows the cracking pattern at peak load for miniatures with diverse a/d (B17, B18, B19, B20, B21, and B22), respectively. For smaller a/d, the staggered spiral stirrups efficiently formed compression strut. For a/d = 1, the crack produced from the point load to the support directly and progressively formed concrete prisms, which crushed when the miniature beam is failed. It is found that the miniature beam failed in pure shear.

Spiral stirrups have extra influence on peak loads with greater a/d ratios. Using spiral stirrup increases the confinement of concrete. The cracking load is influenced in a wide

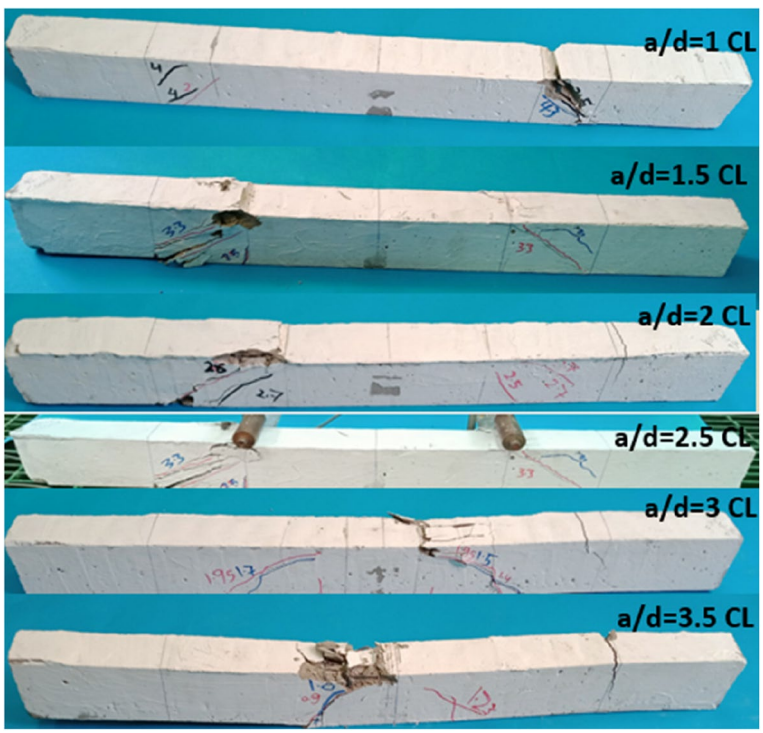

Fig. 11 Cracking propagation of normal stirrups for B11, B12, B13, B14, B15, and B16

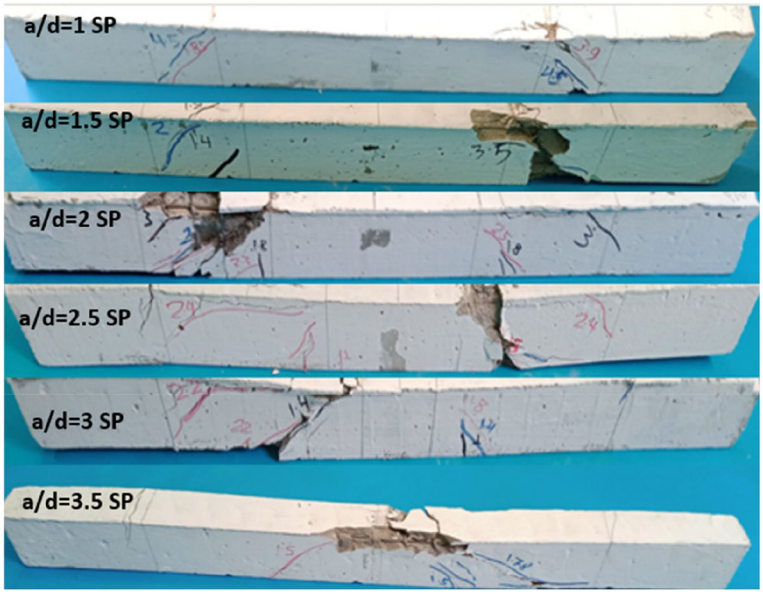

Fig. 12 Cracking pattern of spiral stirrup for B17, B18, B19, B20, B21, and B22

domain compared to the failure load. Once using spiral stirrups as transverse reinforcement, the increment in the cracking load was about 33%. Furthermore, the registered cracking load was higher for miniature with small a/d ratios. This may be traced to the lessening in the bending moment generated for such miniature. Regarding the cracking angle, it is revealed that the crack angle of the spirally stirrups beam is lightly smaller than the crack angle of the corresponding beam with ties.

With higher a/d ratios, spiral stirrups have a greater influence on peak loads. Using spiral stirrups helped to increase concrete confinement. In comparison to the failure load, the cracking load is influenced over a much larger domain. The cracking load increased by approximately 33% when spiral stirrups were used as transverse reinforcement. Furthermore, for miniature with small a/d ratios, the registered cracking load was higher. This could be attributed to a reduction in the bending moment generated by such a miniature. The crack angle of the spirally stirrups beam was found to be slightly smaller than the crack angle of the corresponding ties beam.

For a/d = 3.5, the crack initiated in the miniature web at a shear load of 10 kN, and then new cracks were produced from the lower fiber and extended to the point load. The behavior was more ductile as shown in Fig. 12. As the shear arm ratio increased until 3.5, the equivalent failure mode of RC beams is flexural shear failure.

Analytical predictions

The observed value of the max load P_{max}, the extreme shear strength, $V_u = \frac{P_{max}}{2}$, the shear stress $v = \frac{V_u}{bd}$, and deformation to the extreme load measured in the experiment are also indicated. The predicted shear strength is calculated using various code guidelines, such as the following: Niwa, ACI-318, Eurocode-2, Zararis, British standard, and Canadian Standards Association. Table 5 depicts the test results for

Table 5 Showing test results for miniatures and prototype from B1 to B10

Specimen	Results for miniatures		Results for prototype	
	Shear capacity (kN)	Deflection at max load (mm)	Shear capacity (kN)	Deflection at max load (mm)
B1	9.20	5.8	307.2	46.4
B2	8.20	6.0	273.8	48.0
B3	8.0	5.6	267.13	46.4
B4	7.75	4.0	258.78	32.0
B5	6.20	3.8	207.03	30.4
B6	11.70	9.0	434.1	72.0
B7	10.95	8.0	406.3	64.0
B8	9.0	6.3	333.91	50.4
B9	8.60	4.5	319.1	36.0
B10	7.50	4.2	278.3	33.6

Table 6 Showing test results for miniatures and prototype from B11 to B22

Specimen	Results for miniatures		Results for prototype	
	Shear capacity (kN)	Deflection at max load (mm)	Shear capacity (kN)	Deflection at max load (mm)
B11	21	3.0	701.22	24
B12	17	3.8	567.65	30.4
B13	13.7	4.5	457.46	36
B14	12	5.5	400.69	44
B15	10	5.8	333.91	46.4
B16	6.50	7.5	217.04	60
B17	23	4.8	853.3	38.4
B18	18	5.2	667.83	41.6
B19	15.70	5.3	582.49	42.4
B20	12.50	6.2	463.77	49.6
B21	11	7.7	408.12	61.6
B22	9.2	8.0	341.33	64

Table 7 Comparison of prototype results and calculated estimation according to ECP2020, JSCE 15, and Eurocode-2 for the specimens from B1 to B10

Beam name	Test results	ECP2020		JSCE 15		Eurocode-2	
	$V_{u,Exp}$	$V_{u,ECP}$	$\frac{V_{u,Exp}}{V_{u,ECP}}$	$V_{u,JSCE}$	$\frac{V_{u,Exp}}{V_{u,JSCE}}$	V_{EC2}	$\frac{V_{u,Exp}}{V_{u,EC2}}$
B1	1.70	1.28	1.33	1.30	1.31	1.35	1.26
B2	1.50	1.12	1.34	1.21	1.24	1.247	1.21
B3	1.46	1.01	1.45	1.16	1.26	1.18	1.24
B4	1.41	0.95	1.50	1.12	1.26	1.139	1.25
B5	1.15	0.84	1.40	1.05	1.10	1.06	1.10
B6	2.133	1.28	1.70	1.30	1.64	1.35	1.60
B7	2	1.12	1.80	1.21	1.653	1.247	1.61
B8	1.65	1.01	1.63	1.16	1.422	1.18	1.39
B9	1.57	0.95	1.55	1.12	1.40	1.139	1.40
B10	1.37	0.84	1.63	1.05	1.31	1.06	1.30

Table 8 Comparison of prototype results and calculated estimation according to Niwa model, ACI-318, and Zararis model for the specimens from B1 to B10

Beam name	Test results	Model of Niwa		ACI38-19		Zararis	
	$V_{u,Exp}$	$v_{u,N}$	$\frac{v_{u,Exp}}{v_{u,N}}$	vu, ACI	$\frac{v_{u,Exp}}{v_{u,ACI}}$	vu, z	$\frac{v_{u,Exp}}{v_{u,z}}$
B1	1.70	1.3	1.31	1.55	1.10	1.173	1.45
B2	1.50	1.19	1.1	1.45	1.05	1.10	1.36
B3	1.46	1.13	1.30	1.37	1.06	1.005	1.453
B4	1.41	1.09	1.3	1.30	1.07	0.963	1.464
B5	1.15	1.02	1.15	1.15	1	0.930	1.236
B6	2.133	1.3	1.64	1.57	1.36	1.173	1.818
B7	2	1.19	1.68	1.45	1.38	1.10	1.818
B8	1.65	1.13	1.46	1.37	1.20	1.005	1.642
B9	1.57	1.09	1.44	1.30	1.19	0.963	1.630
B10	1.37	1.02	1.35	1.15	1.20	0.930	1.473

Table 9 Comparison of prototype results and calculated estimation according to Niwa model, ACI-318, and Zararis model for the specimens from B11 to B22

Beam name	Test results	Model of Niwa		ACI38-19		Zararis	
	$V_{u,Exp}$	$v_{u,N}$	$\frac{v_{u,Exp}}{v_{u,N}}$	vu, ACI	$\frac{v_{u,Exp}}{v_{u,ACI}}$	vu, z	$\frac{v_{u,Exp}}{v_{u,z}}$
B11	3.83	1.89	2.03	1.602	2.39	1.75	2.164
B12	3.10	1.57	1.975	1.57	2.0	1.77	1.72
B13	2.50	1.41	1.77	1.55	1.61	1.78	1.36
B14	2.20	1.3	1.70	1.547	1.42	1.80	1.422
B15	1.824	1.26	1.48	1.54	1.18	1.81	1.02
B16	1.20	1.2	1.0	1.50	0.8	1.82	0.7
B17	4.19	1.89	2.217	1.602	2.615	1.75	2.40
B18	3.30	1.57	2.10	1.57	2.10	1.77	1.86
B19	2.88	1.41	2.04	1.55	1.86	1.78	1.62
B20	2.30	1.3	1.80	1.547	1.49	1.80	1.30
B21	2.01	1.26	1.60	1.54	1.31	1.81	1.12
B22	1.70	1.2	1.42	1.50	1.12	1.82	0.95

miniatures and equivalent prototype beams from B1 to 10. Table 6 depicts the test results for miniatures and equivalent prototype beams from B11 to 22. Table 7 shows comparison of prototype results and calculated estimation according to ECP2020, JSCE15, and Eurocode-2 for the specimens from B1 to B10. Tables 8 and 9 show comparison of prototype results and calculated estimation according to Niwa model, ACI-318, and Zararis model for the specimens from B1 to B22.

Design provisions of Eurocode (EC2-04) []

The EC2 2004 formula takes the shear strengthening and concrete attributions in shear resistance, where concrete shares with the beam capacity. The EC2 2004 shear capacity is showing in the following equations. Where $v_{Rd,c}$ is the non-shear RFT design shear strength,$v_{Rd,s}$ is the design shear force presented by shear RFT,$v_{Rd,}$ is the maximum shear force that the sample can withstand, $v_{Ed}is$ the external load-generated

design shear force, α the angle created by the VL ties and the beam axis, ɵ the angle of the strut and the beam axis perpend to the load, A_{sw} the shear RFT area, S the stirrups spacing, f_{ywd} the yield strength of the shear RFT, and v_1 strength reduction factor for concrete cracked in shear. When $v_{Ed} \leq v_{Rd,c}$, there is no need to calculate the shear reinforcement. When $v_{Ed} > v_{Rd,c}$, adequate shear reinforcement must be supplied to make $v_{Ed} \leq v_{Rd,c}$.

$$v_{Rd} = v_{Rd,c} + v_{Rd,s} \tag{1}$$

$$v_{Rd,c} = [\ C_{Rd,c}\, k(100\, \rho_l\, f_{ck})^{1/3}\ ]\ b\ d \tag{2}$$

$$V_{Rd,s} = \frac{A_{sw}}{S} z f_{ywd} (cot\ cot\theta + cot\ cot\alpha) sin\ sin\ \alpha \tag{3}$$

$$V_{Rd,max} = \frac{\alpha_{cw}\, b_w v_1 f_{cd}}{(cotcot\theta + tantan\theta)} 0.9d \tag{4}$$

$$K = 1 + \sqrt{\frac{200}{d}} \leq 2\ ,\ \rho_l = \frac{Asl}{bd}\ ,\quad C_{Rd,c} = 0.18\ ,\ z = 0.9\ d$$

Design provisions of ACI building code (ACI 318–19) []

The shear strength is computed using the average shear stress across the section b_w. d. Shear is presumed to be supported by the concrete in the element without shear RFT. A part of the shear strength is presumed to be provided by concrete and rest by the shear RFT. V_c is the concrete's shear strength. V_s denotes the shear strength supplied by shear.λ = mechanical properties modification factor.

$$v_c = 0.16 \sqrt{f_c} + 17 \frac{\rho_l \frac{d}{a}}{} \tag{5}$$

$$v_s = \rho_t\, f_{ytrans}\ sin\ sin\ \phi \tag{6}$$

$$v_n = v_c + v_s \tag{7}$$

Theoretical formula of Niwa for slender beams []

When an RC beam with ties drop in shear, Eq. (9) commonly expects the maximum load. The shear capacity made by shear reinforcement is given by Eq. (8). The concrete shear capacity is given by Eq. (10) (Niwa 1986). These equations were implemented to regular reinforced concrete beams. Where a shear span, d beam depth, b_w width, S tie spacing, and z distance between the compression and tension forces, as main RFT area, A_w tie area, f_c concrete strength, and f_{wy} tie yield strength.

$$v_s = \frac{A_{web} f_{wy} z}{s} \tag{8}$$

$$v_c = 0.2[100 f'_l f_c]^{\frac{1}{3}} [\frac{1000}{d}]^{\frac{1}{4}} [0.75 + \frac{1.4}{\frac{a}{d}}] bd \tag{9}$$

$$2v_u = 2(v_s + v_c) \tag{10}$$

Japan standard specification (JSCE 2007) []

Equation (11) is used to evaluate the design elements' shear capacity in the absence of shear RFT. When both longitudinal and ties are used as shear RFT, the design shear capacity of an element could be determined via Eq. (12). It should be made sure that the ties provided carries at least half the shear force supplied by shear RFT. Where α angle of VL ties and beam axis, A_{sw} area of shear RFT, S ties spacing, and f_{ywd} the shear RFT yield strength.

$$v_{cd} = \left(\sqrt[4]{\frac{1000}{d}}\right)\left(\sqrt[3]{100 \times \frac{A_s}{bd}}\right)\left(0.2\sqrt[3]{f_{cd}}\right) \cdot b_w \cdot \frac{d}{1.3} \tag{11}$$

$$v_{sd} = [A_w f_{ywd} (sin\, sin\, \alpha_s + cos\, cos\, \alpha_s)/s_s] \frac{z}{1.1} \tag{12}$$

$$v = v_{cd} + v_{sd} \tag{13}$$

Theoretical formulation of Zararis for slender beams []

$$v_{u,z} = \lambda \frac{c}{d} f_{ct} + (0.5 + 0.25 \frac{a}{d}) f'_t f_{yt} \tag{14}$$

$$\frac{c^2}{d^2}+600\frac{f'_l+f_t}{f_c}\cdot\frac{c}{d}-600\frac{f'_l+\frac{d'}{d}f'_l}{f_c}=0 \tag{15}$$

λ: size effect coefficient presented by the expression $\lambda = 1.2–0.2a \geq 0.65$ [a: shear span], f_{ct}: the splitting tensile strength of concrete $f_{ct} = 0.3\ f_c^{\frac{2}{3}}$, and c: the compression zone depth.

ECP 203–20

According to ECP 203, shear stress should be conveyed by concrete and shear RFT contribution. The permissible shear stress in *MPA* is shown in Eq. of q_{cu}. ECP 203–07 calculates the shear stress caused by vertical load. Shear stress due to vertical load is shown in equation of q_{su}, and shear stress due to direct shear is shown in equation of q_u.

$$q_{cu}(cracked) = 0.12\sqrt{\frac{f_{cu}}{1.5}} \tag{16}$$

$$q_{su}=\frac{A_{st}\frac{f_{ys}}{1.15}}{bs} \tag{17}$$

$$q_u = q_{cu} + q_{su} \tag{18}$$

Dissipated energy

The area under the shear load–deflection curves until the highest load is calculated to assess the energy dissipated. The relation between dissipated energy and stirrup's spacing is depicted in Fig. 13. It is demonstrated that the miniatures strengthened with spiral stirrups had the most dissipated energy compared to the other miniatures. When the tie

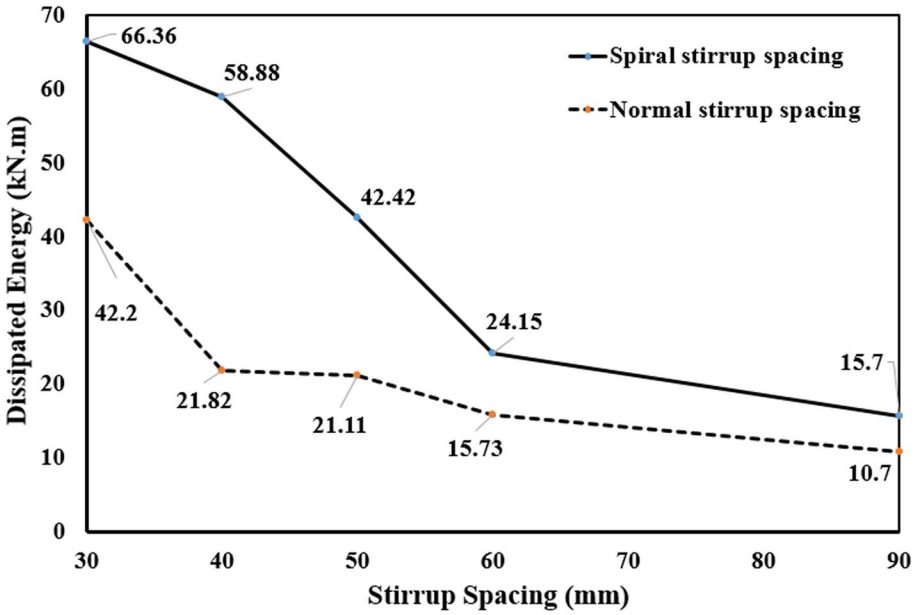

Fig. 13 The relationship of the dissipated energy and the ties spacing

spacing, S, is reduced, the dissipated energy increases. The results display that the most dissipated energy of 66 kN.m occurs at spiral stirrups spacing $S = 30$ mm for miniature B6. Spiral stirrups can be applied to boost the miniature's shear resistance. Figure 14 depicts the dissipated energy versus the shear span arm ratio, a/d. By increasing the shear span arm ratio, a/d, the deformations at peak load increase slightly and hence the dissipated energy. Closer stirrups spacing is thought to firmly close diagonal cracks and experience large deformations when compared to larger tie spacing. Given that both can delay shear failure, the closer spacing may result in better deformations.

Contribution of the staggered spiral stirrups

The results obviously demonstrate that the application of staggered spiral ties boosted shear capacity and shear mechanism in the investigated beams. Miniature beams with 30-mm and 40-mm continuous staggered spiral reinforcement spacing showed 33% and 27%, respectively, boosted shear capacity in comparison to normal ties. The spiral ties create an additional confinement that increases the concrete capacity for shear transfer and the concrete compressive strength. The increased concrete compressive strength caused by the spiral confinement would cause an increase in the outset of the shear cracking. As a result, the staggered spirally reinforced beams display a considerable increase in shear strength when compared to normal ties.

A comparison between two RFT techniques in terms of weight

To evaluate the efficacy of two techniques, the strength of RFT for every technique is assessed in all studied cases. The strength and weight of all stirrups are compared. Figure 15 shows the weight of stirrups and stirrup spacing for each shear reinforcement technique for diverse stirrup spacing. The greatest strength was achieved by using spiral stirrup, but the highest weight was achieved by using separate ties. It can be concluded that the staggered spiral ties demonstrated the greatest strength and thus may be considered the most efficacious reinforcement

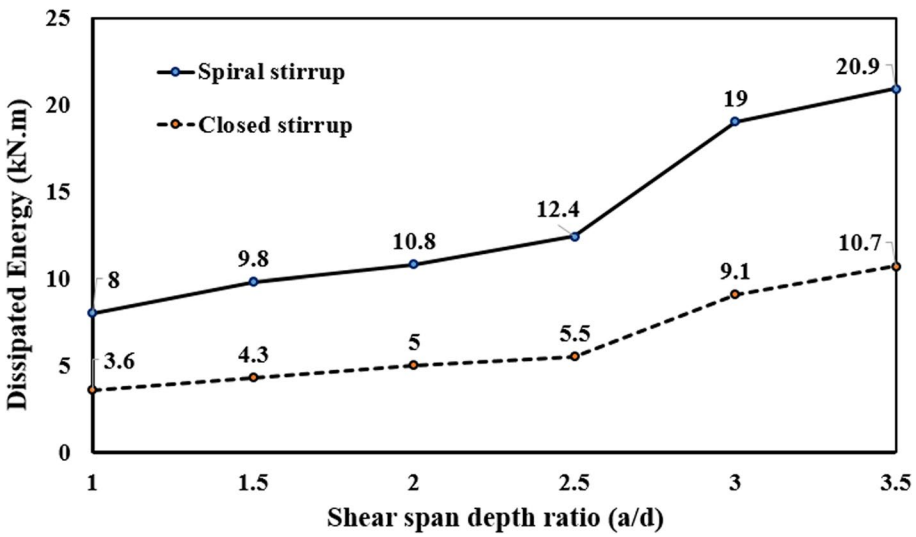

Fig. 14 The dissipated energy and the span depth ratio

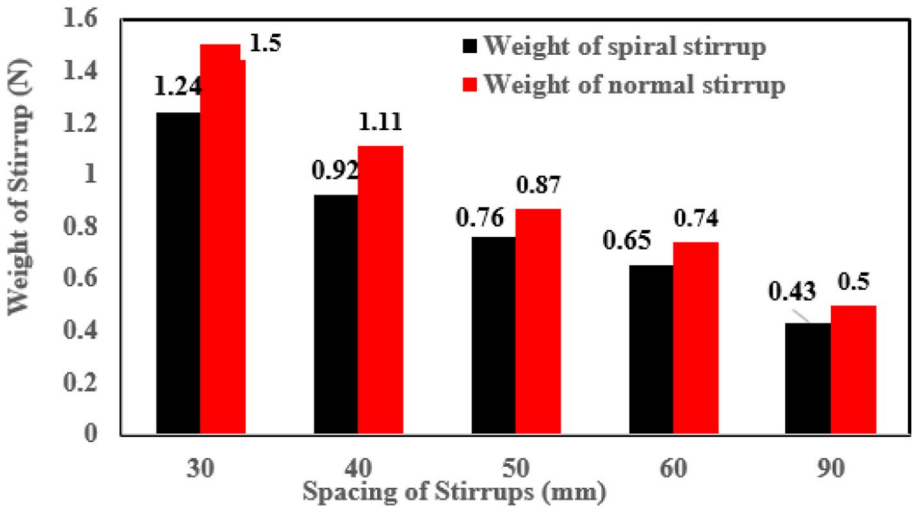

Fig. 15 The relationship of the stirrup weight and stirrup spacing

technique for shear of miniatures beams. To obtain a shear capacity of 267.13 kN, staggered continuous spiral with consecutive spacing of 400 mm is used instead of separate ties with successive spacing of 250 mm, as it is more economical in addition to saving in volume of stirrups 53%. For getting the ductility of 46, staggered continuous spiral successive spacing of 400 mm is used instead of separate ties with successive spacing of 320 mm, as it is more economical and saves steel weight. To evaluate the efficacy of different methodologies, the weight of transverse RFT pattern is assessed for each RFT pattern in all inspected miniatures. Weight is calculated for all studied miniatures for each technique. Spiral stirrups had the lowest weight, so they may be considered the most effectual transverse RFT technique for shear beam.

Adjusting the results from the small scale to the prototype

By connecting the data, the experimental scale-down results are converted into prototype full-scale behavior. Because the model and the prototype are related, the small model's results will be interpreted in order to expect the prototype behavior. The goal of this study is to get full-scale design information by connecting data from the scaled-down model. The connection between the large and small scales is also shown. The steel's stress similitude has been kept, whereas f_{ymodel} is 690 N/mm^2 as opposed to f_{yproto} is 360 N/mm^2. We can reduce the ties volume while maintaining the performance by using staggered continuous ties instead of normal ties, and the greater the shear capacity and dissipated energy, the smaller the stirrups spacing. Staggered continuous spiral covers a larger size, and therefore, whenever a crack arises, it changes its path. Therefore, the crack surface increases and takes more time. The form of staggered continuous spiral packs the beam with a larger surface. The equivalent prototype section is (f_{yproto} = 360 N/mm^2), B × d = 40 × 57 cm, beam length = 6.0 m, tensile reinforcement 4ϕ20, compressive reinforcement 2 ϕ12, ties ϕ = 8 mm, and Fcu = 40 Mpa. The relation of shear capacity with stirrups spacing is displayed in Fig. 16. The relation of deflection at max load and stirrups spacing is displayed in Fig. 17. The relation of

shear capacity with shear arm ratio is displayed in Fig. 18. The relation of deflection at peak and shear arm ratio is displayed in Fig. 19.

$$\frac{Load_{prototype}}{Load_{model}} = Scale^2 \frac{f_{yprototype}}{f_{ymodel}} \tag{19}$$

Comparisons between experimental results and codes

Design code equations are always conservative because they take a margin of safety into account. All code formulations (JSCE 15, CSA A23.3, ACI318-19, Eurocode, and ECP 2020) are conservative in guessing the shear capacity of RC beams with normal transverse RFT. The calculated ultimate shear capacity of most of design codes is slightly lower than the experimental results for normal ties as shown in Figure 20, but for spiral ones, the calculated values are relatively more conservative as shown in Figure 21. Design codes mostly do not consider the continuity of spiral ties in forecasting shear capacity, while its influence found significant in the experimental results. So, effect of spiral continuity confinement should be considered in design. Size effect is minimized by using mortar instead of concrete.

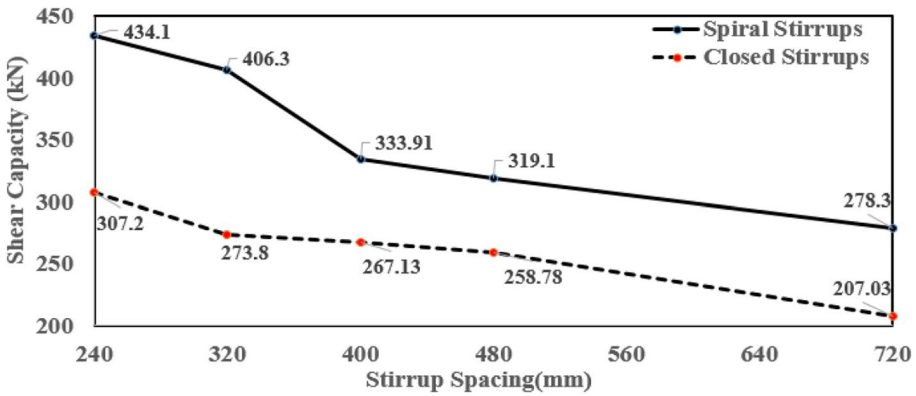

Fig. 16 Shear capacity and stirrup spacing for prototype for normal and spiral stirrups

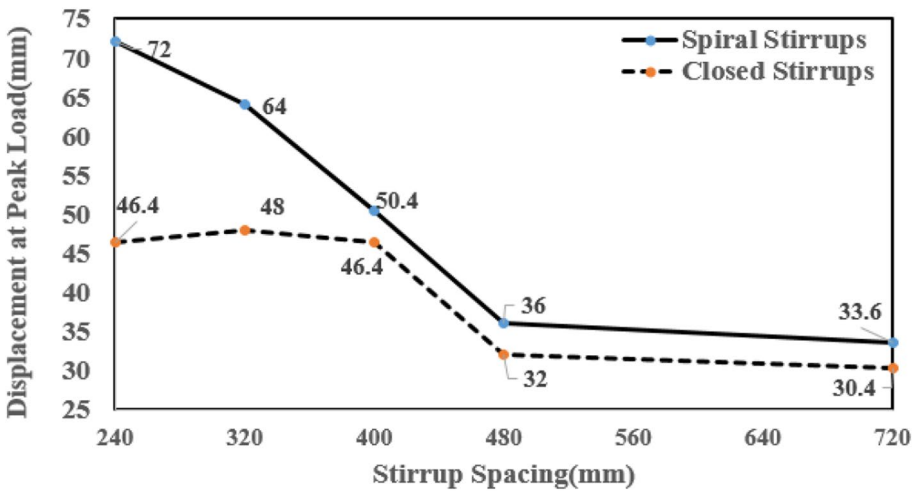

Fig. 17 Deflection at max load and stirrup spacing for normal and spiral stirrups

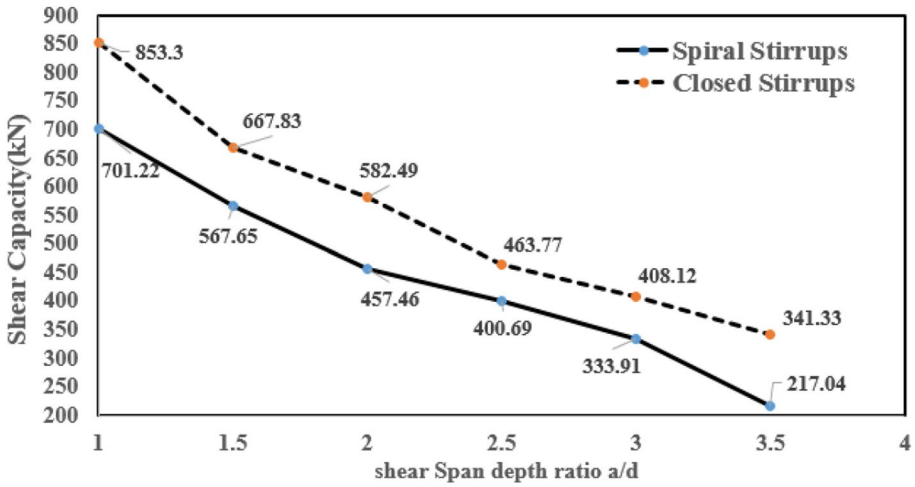

Fig. 18 Shear capacity and a/d for prototype for normal and spiral stirrups

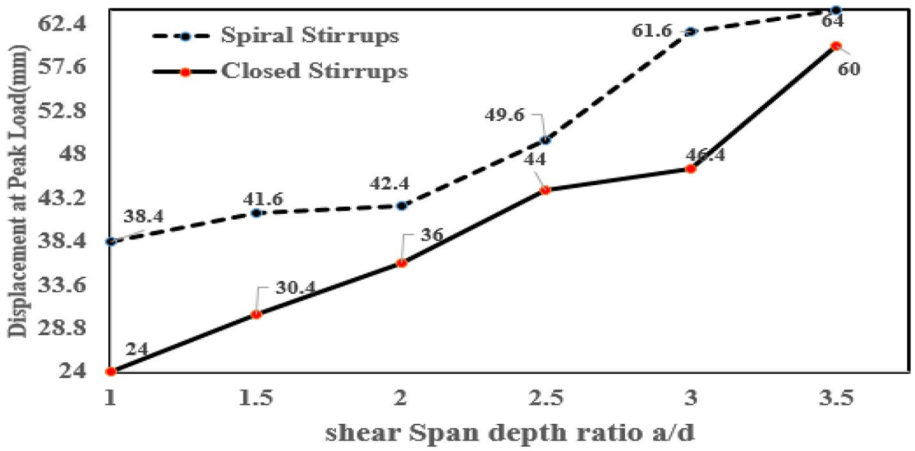

Fig. 19 Deflection at max load and a/d for prototype for normal and spiral stirrups

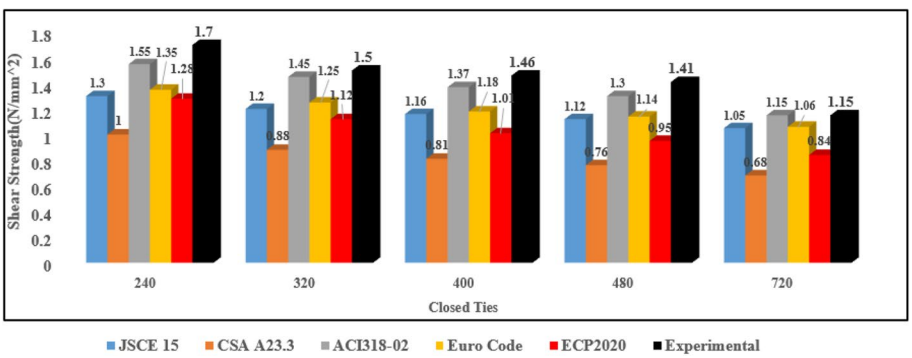

Fig. 20 JSCE 15, CSA A23.3, ACI318-02, Eurocode, ECP 2020, and test result for separate ties

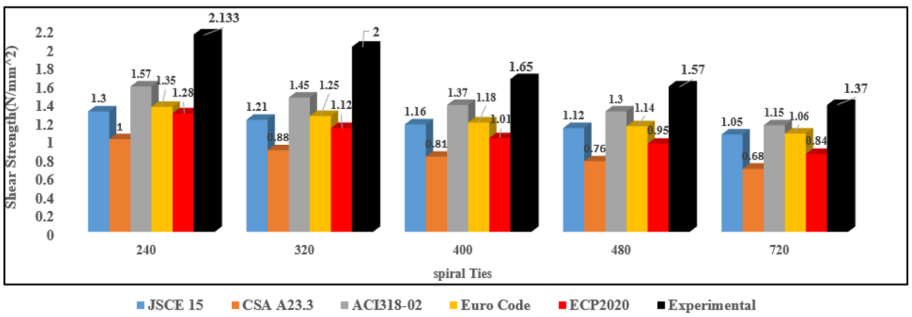

Fig. 21 JSCE 15, CSA A23.3, ACI318-02, Eurocode, ECP 2020, and test result for spiral ties

Conclusions

The current study used scaled-down modelling as an experimental approach to investigate the shear behavior of specimens with normal ties and rectangular staggered continuous spiral ties. Twenty-two rectangular miniatures with identical reinforcement detailing were tested in shear until they collapsed. The purpose was to evaluate the effectiveness of spiral ties as internal transverse RFT. The following conclusions are drawn:

1. The application of staggered spiral ties increased shear capacity and improved shear behavior in the investigated beams.
2. Beams with staggered continuous spiral ties at spacing of 30 mm and 40 mm increased shear capacity by 33% and 27%, respectively, when compared to normal ties.
3. Because spiral ties are continuous, an additional confinement arises that improves concrete compressive strength and predictably increases concrete capacity for shear transfer.
4. Specimens reinforced with spiral ties have larger diagonal cracks zone, but specimens reinforced with separate ties have localized diagonal cracks.
5. Spiral hooks effectively reduced the crack width compared to conventional ties. This could be due to the continuity of spirals along the beam, which bridge cracks along concrete perimeter.
6. The spiral confinement would lead to a rise in shear load at the shear cracking onset. The experiments reveal that the staggered spirals confinement contribution is responsible for the increase in peak shear capacity.
7. Relying on these comparisons, it is obvious that the design provisions of EC2-04, ECP 203–20, and ACI 318–19 are conservative in assessing the peak shear strength of the beams within a reasonable margin.

Abbreviations

RC	Reinforced concrete
D	Depths of specimen
LVDT	Load variable differential transducers
RFT	Reinforcement
F_u	Ultimate stress of rebar
F_y	Rebar reinforcement yield stress
E	Material Young's modulus
F_{cu}	Cube compressive stress at age 28 days
ε	Strain of rebar
SDM	Scale-down modelling
a/d	Shear span arm ratio a/d

Acknowledgements
Not applicable

Authors' contributions
All authors read and approved the final manuscript.

Funding
Not applicable.

Availability of data and materials
The data can be shared upon request as a basic requirement dictated by Springer rules.

Declarations

Competing interests
The authors declare that they have no competing interests.

Received: 2 December 2023 Accepted: 3 February 2024
Published online: 27 February 2024

References

1. Seo JM, Choi IK (2000) Review of ultimate pressure capacity test of containment structure and scale model design techniques
2. Mahmoud S, Youssef A, Salem H (2022) Enhanced torsion mechanism of small-scale reinforced concrete beams with spiral transverse reinforcement. Civ Eng J 8(11):2640–2660. https://doi.org/10.28991/CEJ-2022-08-11-019
3. Majorana CE, Salomoni VA, Mazzucco G, Pomaro B, Xotta G. (2015). Mechanical modelling of concrete and concrete structures. https://doi.org/10.4203/ctr.11.1
4. Mohammed AMY, Maekawa K (2012) Global and local impacts of soil confinement on RC pile nonlinearity. J Adv Concr Technol 10(11):375–388. https://doi.org/10.3151/jact.10.375
5. Carpinteri A, Corrado M (2010) Dimensional analysis approach to the plastic rotation capacity of over-reinforced concrete beams. Eng Fract Mech 77(7):1091–1100. https://doi.org/10.1016/j.engfracmech.2010.02.021
6. Christianto D, Makarim CA, Liucius YU (2020) Size effect on shear stress of concrete beam without coarse aggregate. In Journal of Physics: Conference Series (Vol. 1477, No. 5, p. 052043). IOP Publishing https://doi.org/10.1088/1742-6596/1477/5/052043
7. Shatarat N, Katkhuda H, Alqam M (2016) Experimental investigation of reinforced concrete beams with spiral reinforcement in shear. Constr Build Mater 125:585–594. https://doi.org/10.1016/j.conbuildmat.2016.08.070
8. Joshy V, Faisal KM (2017) Experimental study on the behaviour of spirally reinforced SCC beams. Int J Eng Res General Sci 5(3):96–105 ISSN 2091–2730
9. Megahid AER, Rashwan MM, Mahmoud M, El Aal AA (2016) Effect of shear span to depth ratio on the statical behavior of hscb subjected to transverse loading. JES Journal of Engineering Sciences 44(1):1–26. https://doi.org/10.21608/jesaun.2016.110663
10. Hua B, Wu YF (2018) Effect of shear span-to-depth ratio on shear strength components of RC beams. Eng Struct 168:770–783. https://doi.org/10.1016/j.engstruct.2018.05.017
11. Meghana BM, Neena V (2018) Shear capacity of RC beams with different patterns of spiral reinforcements. Int J Eng Res Technol (IJERT) ETCEA 6
12. Suman TalapaReddy, Sreevalli IY (2020) Numerical study on flexural performance of RC beam with various confinement pattern. Eng Res Express 2(1):015016. https://doi.org/10.1088/2631-8695/ab68a3
13. Dewi SH & Thamrin, R. (2020). Effect of stirrup type on shear capacity of reinforced concrete members with circular cross section. In E3S Web of Conferences (Vol. 156, p. 05022). EDP Sciences. https://doi.org/10.1051/e3sconf/202015605022
14. Azimi M, Bagherpourhamedani A, Tahir MM, Bin Mohd Sam AR, Ma CK (2016) Evaluation of new spiral shear reinforcement pattern for reinforced concrete joints subjected to cyclic loading. Adv Struct Eng 19(5):730–745. https://doi.org/10.1177/1369433216630371
15. ACI Committee (2019) Building code requirements for structural concrete (ACI 318–19) and commentary. American Concrete Institute
16. JSCE (2007) Standard specifications for concrete structures-2007, Design. Japan Society of Civil Engineers, Tokyo (Japan)
17. Code, P. (2005). Eurocode 2: design of concrete structures-part 1–1: general rules and rules for buildings. British Standard Institution, London. Ref. No. EN 1992–1–1:2004: E
18. Zararis PD (2003) Shear strength and minimum shear reinforcement of reinforced concrete slender beams. Struct J 100(2):203–214. https://doi.org/10.14359/12484
19. Niwa J, Yamada K, Yokozawa K, Okamura H (1986) Revaluation of the equation for shear strength of reinforced concrete beams without web reinforcement. Doboku Gakkai Ronbunshu 1986(372):167–176. https://doi.org/10.3151/jact.12.187
20. Egyptian Code of Practice (2020) Ministry of Housing, Utilities and Urban Communities, Egyptian code for design and construction of reinforced concrete structures (E 203–2020)

Publisher's Note